
Regional Ventilation and Lung Mechanics Using X-Ray CT¹

Brett A. Simon, MD, PhD

Advances in computed tomographic (CT) imaging of the lung in the past decade, particularly with increased speed, resolution, gating capability, and rapidly expanding volumetric image acquisition, along with advances in image processing, have expanded the repertoire of imaging methods beyond anatomic visualization into the noninvasive study of regional lung physiological function. Recognizing that significant local disease or dysfunction can exist before global measures begin to deteriorate, the motivation for the development and application of these regional techniques is to further our understanding of the basic pathophysiological characteristics of evolving lung disease and, ultimately, develop sensitive measures for its early detection. This review emphasizes the key elements of ventilation and lung mechanics relevant for regional approaches and CT measurement principles available for their study. Examples of established and evolving methods for imaging regional ventilation and mechanics, including the xenon CT ventilation method; the relationship between changing regional CT density and air volume change; and registration-based methods for examining regional lung expansion and strain, are presented.

© AUR, 2005

Whereas x-ray computed tomography (CT) has long provided important documentation of the anatomic evidence of lung disease, its use in the late 1980s to define the heterogeneous mechanical nature of acute lung injury and a pathophysiological rationale for management strategies (1–5) marked a transition into the era of functional lung imaging. Advances in CT imaging of the lung in the past decade, particularly with increased speed, resolution, gating capability, and rapidly expanding volumetric image acquisition, along with requisite advances in image processing, have expanded the repertoire of imaging methods beyond anatomic visualization into the

noninvasive study of regional lung physiological function. Recognizing that significant local disease or dysfunction can exist before global measures begin to deteriorate, the motivation for the development and application of these regional techniques is to further our understanding of the basic pathophysiological characteristics of evolving lung disease and, ultimately, develop sensitive measures for its early detection. This review emphasizes the key elements of ventilation and lung mechanics relevant for regional approaches and CT measurement principles available for their study. Examples of established and evolving methods for imaging regional ventilation and mechanics are presented.

Acad Radiol 2005; 12:1414–1422

¹ Department of Anesthesiology, Tower 711, Johns Hopkins Hospital, Baltimore, MD 21287-8711; Departments of Critical Care Medicine and Medicine, The Johns Hopkins University, Baltimore, MD. Received April 4, 2005; revision received July 25; revision accepted July 27. Presented at the 2004 International Workshop on Pulmonary Imaging at Penn, Philadelphia, PA, November, 12-14 2004. Supported in part by Department of Defense DAMD 17-02-1-0732 and grant no. HL64368 from the National Institutes of Health. **Address correspondence to:** B.A.S. e-mail: bsimon@jhmi.edu

© AUR, 2005

doi:10.1016/j.acra.2005.07.009

VENTILATION

To a physiologist, ventilation is the process by which fresh gas is transferred to the alveoli, resulting in replenishment of oxygen, removal of carbon dioxide, and, in the presence of blood flow, exchange of these gases with the subject. This is a steady-state dynamic process. Alveolar

ventilation, the portion of total ventilation that contributes to gas exchange, determines arterial P_{CO_2} and reflects the net contribution of all lung units. Distribution of ventilation within the lung depends on many factors, including airway resistance and branching patterns, regional lung compliance, flow rates, lung volume, regional pleural pressure changes, and gas properties. Ventilation distribution also is regulated actively on a local level in concert with perfusion to optimize gas exchange.

Physiologists have used indirect methods to make inferences about the distribution of ventilation or ventilation-perfusion (V/Q) matching by examining, for example, the concentration profile of nitrogen in single-breath or multibreath washout procedures (6) or the multiple inert gas elimination technique (7). However, imaging methods, initially using planar detectors and radioactive tracer gases (8) and, more recently, tomographic methods (9–12), have provided information on regional lung ventilation. Although certain imaging approaches sometimes are used because of convenience or technological limitations, it is important to emphasize that ventilation distribution is related to, but not the same as, the distribution of aeration, the distribution of a vital capacity or large-volume single breath, and the change in regional lung density over a tidal breath.

LUNG MECHANICS

Broadly, lung mechanics describes the relationship between lung expansion or deformation and applied pressure. The lung and chest wall are constrained to change volume the same amount. Depending on the pressures measured, the mechanics obtained may relate to the lung, chest wall, or respiratory system (lung and chest wall together). The lung expands in response to increases in transpulmonary (alveolar-intrapleural) pressure, but because it is difficult to measure intrapleural pressure, most descriptions of lung mechanics in patients describe respiratory system properties. However, locally, intrapleural pressure depends on many factors, including gravity, body position (supine, prone), chest wall and diaphragm activity, and cardiac motion, and this local pleural pressure determines local lung expansion (13). Even if an estimate of average pleural pressure, using such a device as an esophageal balloon or intrapleural catheter, is used, the local pleural pressure needed for a true measure of regional lung mechanics would not be available.

CT MEASUREMENT PRINCIPLES

CT directly measures only two quantities, density and volume, but it can do so throughout the interior of the object in its view. Density is measured in Hounsfield units (HU), an arbitrary linear scale defined as zero for water and (approximately) -1000 for air. This scale is particularly convenient for lung imaging because the lung is composed of two “materials”: air, at -1000 HU, and “tissue” (eg, blood, water, cells) at approximately 0 HU. (Because exact HU values for air and tissue may vary between scanners and depend on, eg, daily calibration and manufacturer, the best results are obtained by measuring air and tissue reference values from each image set and using those values to scale the data.) Thus, a lung region with a density of -600 HU translates to an average 60% air and 40% tissue; -800 HU translates to 80% air, and so on. Similarly, as lung volume increases, air enters the lung while the tissue component remains relatively constant (plus or minus changes in blood volume); thus, density decreases. Volume is simply the product of the in-plane cross-sectional area of the region of interest (ROI) and slice thickness and can be defined precisely in units of cubic millimeters or milliliters. Finally, absolute volumes of air and tissue in an ROI are obtained from total volume times the fraction of air or tissue.

All functional lung measures involve creative use of these simple principles. Tracer techniques for ventilation use a radiodense gas (xenon [Xe], krypton) as an inhaled contrast agent and standard dye-dilution analyses (14). These methods have the advantage that the accumulation of tracer gas during regular breathing should follow the same gas transport principles as respiratory gases. Density-based methods require the assumption that the decrease in CT density as a region expands is caused by only gas influx. Similarly, registration methods, which follow anatomic tissue deformation (15,16), also must assume that the changes in volume observed occur because of gas influx to estimate ventilation.

Breathing is a dynamic process, and, particularly in diseased or injured lungs with heterogeneous mechanical properties, the distribution of inspired and expired gas has temporal and topographic properties. For example, in lungs in which there are different regional time constants, such as those affected by emphysema, the important difference may be the rate of filling or emptying as opposed to absolute regional volume change (17,18). In this case, the degree of ventilation heterogeneity may be a function

of respiratory rate, and the lung may appear uniform if ventilation is slow or enough time is allowed at end-expiration or end-inspiration. The development of CT scanners with short scan apertures, capable of gated imaging at multiple points in the respiratory cycle during steady-state breathing, enable study of this additional dimension of lung mechanics.

Finally, to properly interpret regional functional imaging data, it is important to pay attention to the denominator used. The lung moves relative to the imaging plane; with full inflation, the base of the lung in a human may displace 3–6 cm caudally. Thus, repeated imaging at a fixed table location, but different lung volumes, may result in the comparison of quantitative measures actually made to different anatomic lung regions. Fortunately, with the high-resolution anatomic detail present in CT images, it is possible to minimize this problem by the matching of distinct anatomic markings to identify nearly the same lung region from image set to image set (19). However, unless three-dimensional (3D) image registration techniques are used (16), comparisons of absolute volume measurements between slice data are susceptible to registration errors, whereas comparisons of density measures (by definition, normalized for regional volume) are more robust. Conversely, whole-lung imaging permits the use of mass balance principles to detect changes in absolute air and tissue volumes without normalization. Similarly, one must distinguish between measurements of absolute ventilation, which is determined externally by respiratory rate and tidal volume, and measurements of ventilation distribution, which better describe relative changes in ventilation between lung regions.

XE-CT VENTILATION IMAGING

The use of Xe gas as an inhaled contrast agent for CT-based regional ventilation measurement was pioneered 25 years ago by Gur et al (12,20), but only recently has the method been updated and applied (21–25). Stable (nonradioactive) Xe gas is denser than air (26–28); thus, the CT density of an airspace containing Xe increases linearly with Xe concentration (Figure 1). By imaging the same lung location in serial end-expiratory gated CT scans as the inspired gas is switched from air to Xe/oxygen and back to air, the rate of increase and decrease in ROI density as Xe washes into and out of the peripheral airspaces can be measured. Assuming a single-compartment model, the time constant of this density-time curve is equal to the

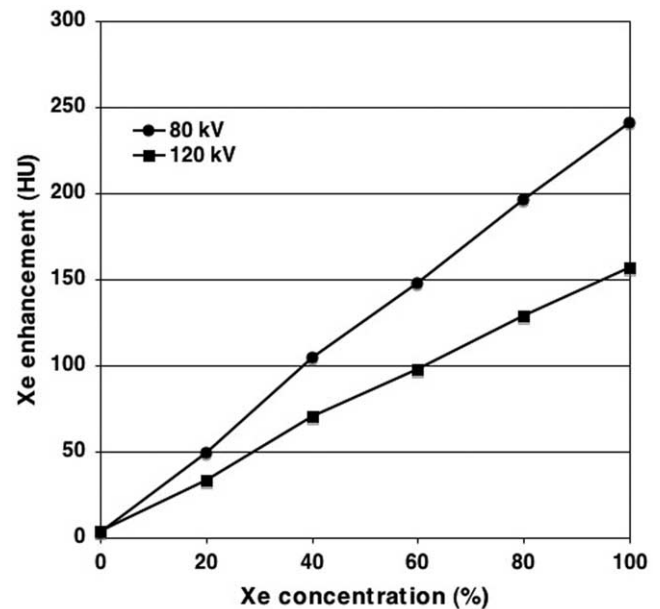


Figure 1. Xe enhancement in HU vs concentration. Note the greater enhancement at lower kV.

inverse of the specific ventilation, the ventilation per unit of gas volume (Figure 2). Using this method, regional ventilation can be mapped for regions with areas as small as 5×5 pixels (Figure 3), although noise caused by partial volume effects, registration of the ROI from image to image, and variations in lung volume are all increased at smaller ROI sizes (24). Each Xe-CT study involves a series of images at a single axial location with whatever volumetric coverage the scanner provides, and multiple repeated studies are needed if larger volumes or different locations are needed. By combining Xe-CT ventilation studies with CT bolus-contrast injection regional perfusion measurements (22,29,30), regional distributions of ventilation, perfusion, and V/Q ratio can be generated as images or continuous distributions. In Figure 4, the fraction of total ventilation at different values of V/Q is plotted as a histogram for the entire lung and for the apex, midlung, and base subvolumes for an anesthetized normal supine sheep. Whole-lung data have a normal mode of 0.89 ± 0.01 ; however, in addition, differences between different lung regions are evident.

Although the Xe-CT method can provide noninvasive high-resolution maps of regional ventilation, there are several important limitations. First, current models assume there is no uptake or recirculation of Xe, washin and washout time constants are equal, and Xe distributes similarly to the respiratory gases oxygen and carbon dioxide.

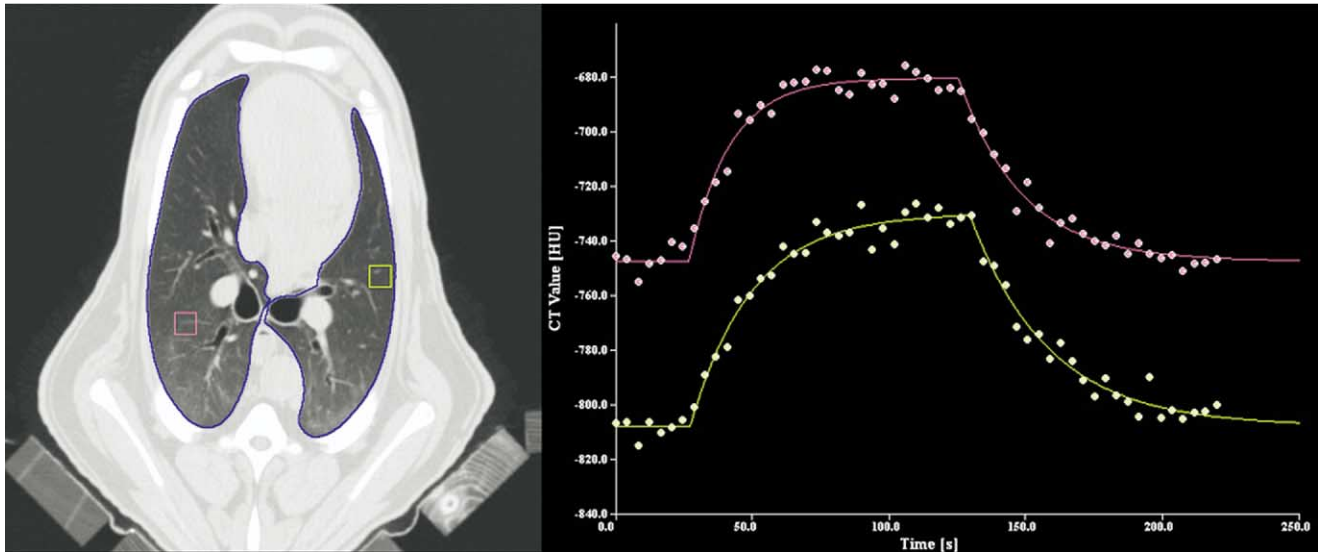


Figure 2. Xe-CT example with density-time curves for two ROIs from a supine, anesthetized, mechanically ventilated sheep.

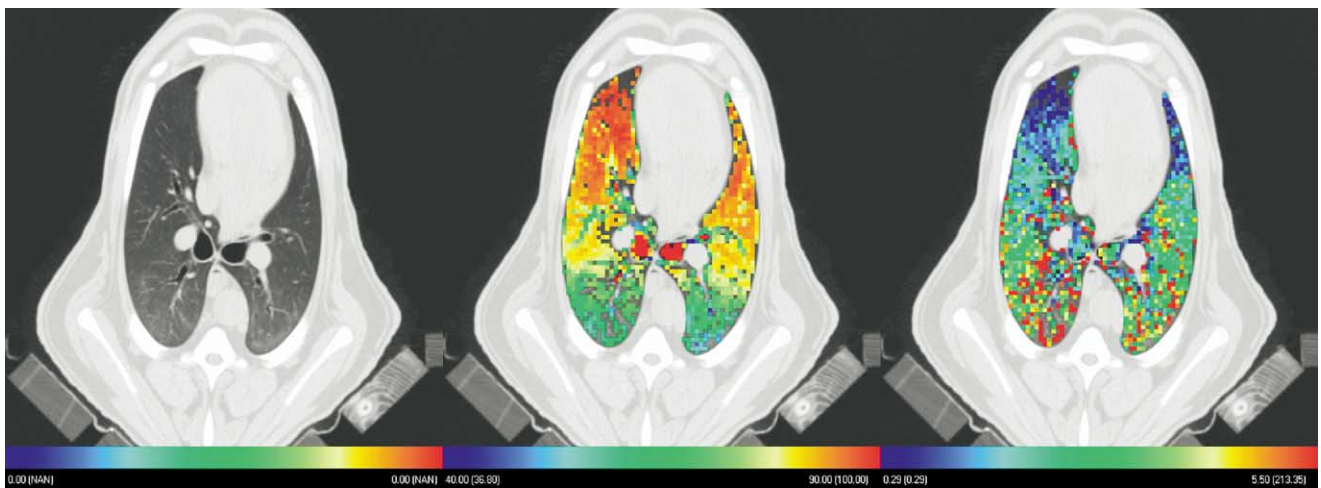


Figure 3. Regional Xe-CT analysis (ROI size, 8×8 pixels) for a slice at the level of the carina, showing (a) original gray-scale image and color maps of (b) regional air content (% air) and (c) specific ventilation (sec^{-1}).

Xe is moderately soluble in blood and is taken up by the circulation: that uptake is the basis for the original use of inhaled Xe and CT imaging for measurement of regional cerebral perfusion (31,32). In addition, uptake of Xe by the pulmonary circulation decreases the maximum alveolar Xe concentration attained during washin; this difference has been used to estimate regional perfusion in addition to regional ventilation (33). Xe has much greater density and viscosity than air; thus, it is possible that its distribution within the lung may depart from the normal respiratory gases, particularly at greater inspiratory flow rates (34).

The signal-to-noise ratio depends on distinguishing the density enhancement of Xe gas from background lung density; thus, it will be decreased by anything that adds noise to the background density (such as breath-to-breath registration errors, partial-volume effects, or changes in lung volume) or increases the background density (such as lung injury or intravenous contrast accumulation). Because inhaled Xe is an anesthetic, approximately 30% more potent than nitrous oxide (35), its use in humans is limited by side effects to 30%–40% (36,37) and ultimately limits the maximum signal achieved. However, the most important limitation for application in patients

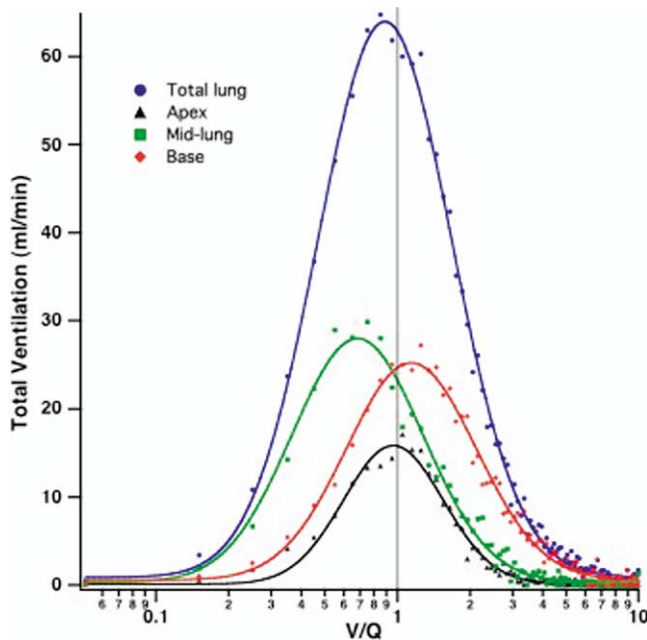


Figure 4. Histograms of total ventilation (mL/min) at different V/Q ratios for the entire lung (blue) and apex (black), midlung (green), and base (red) subvolumes in a supine anesthetized sheep. Ventilation data were obtained from Xe-CT studies and perfusion data from bolus contrast injection studies by Hoffman et al (22).

is that it is time and radiation intensive. Each study requires 20–70 repeated respiratory-gated axial images at each location, with repeated runs to obtain volumetric coverage.

TIDAL LUNG DENSITY CHANGES

Because the decrease in lung density with inflation is caused by the inflow of gas, the density change of an ROI over a tidal breath or with a step change in static airway pressure has been equated with regional ventilation (38,39). However, this relationship is non-linear and dependent on both initial region density and the magnitude of the density change. This effect can be modeled assuming a simple mass balance with conservation of tissue elements and that air and tissue have densities of -1000 and 0 HU, respectively (Figure 5). The specific volume change (sVol; change in volume divided by initial gas volume) for the same change in density can vary threefold as the initial region density changes from -500 to -850 HU, values of lung density found within the normal lung. However, using the same model assumptions, one can show that sVol can

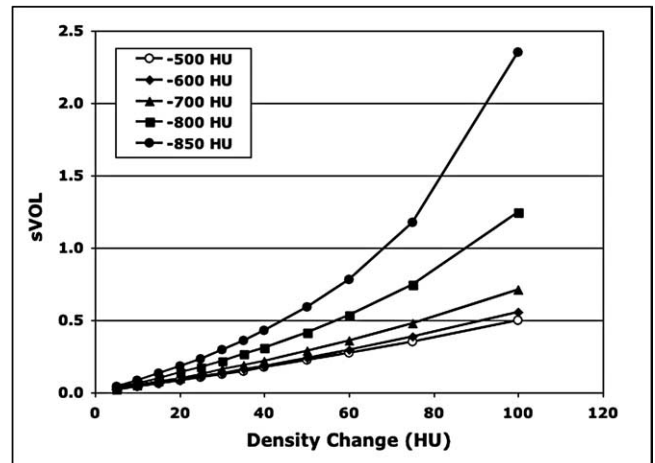


Figure 5. Calculated sVol (volume change/initial air volume) for an ROI as a function of the change in density at different starting densities. Note there can be large differences in sVol for the same ROI density change depending on initial region density, illustrating why CT density change is a poor correlate for regional ventilation.

be calculated from the density change with the following formula (40):

$$\text{sVol} = 1000 (H2 - H1) / (H1[H2 + 1000])$$

Note that ROI volume does not appear in this relationship, only mean ROI density. Assuming that all gas entering the region is fresh gas, sVol should be related closely to specific ventilation. Comparing sVol with specific ventilation measured by means of Xe-CT in a healthy supine sheep, there was a high degree of correlation ($r^2 = 0.73$) for ROI with an average size of 1.6 ± 0.7 mL (41).

There are several advantages to the use of sVol as a surrogate for regional ventilation. First, it requires only two images at different lung volumes. Of course, images obtained with high-speed scanners gated to end-expiration and end-inspiration will better reflect lung dynamic behavior than those obtained during breath-hold imaging. Care should be taken to use the detail in the images to match the same anatomic ROI at different volumes, even if these regions appear in different numbered slices at the different volumes. However, because sVol uses mean ROI density, it should be less sensitive to small registration errors and partial-volume effects than absolute volume measurements. The primary disadvantage of this approach is that it is time consuming if manual ROI matching is used; computer automation and 3D ROI definition will help with this problem, as described next.

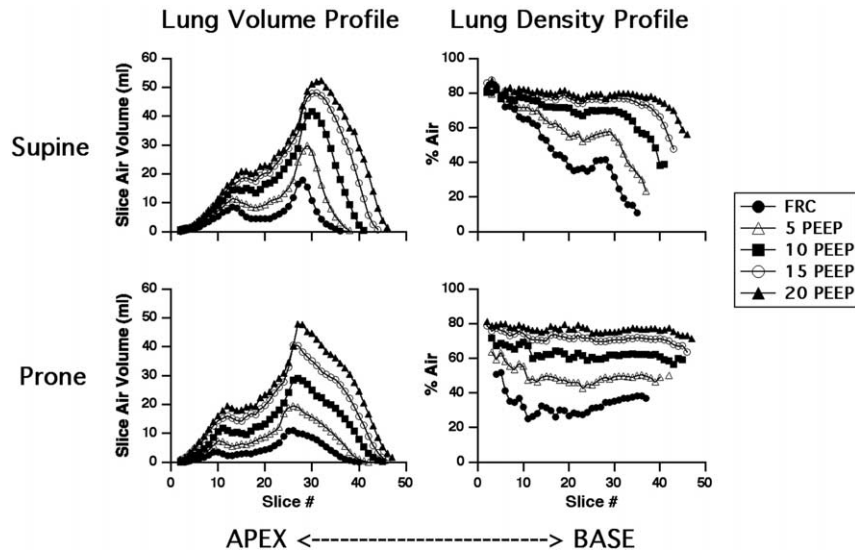


Figure 6. Axial distribution of lung slice air volume and density in a dog after oleic acid lung injury in prone and supine positions and at different PEEP levels. Note the different volume profiles between the prone and supine positions, resulting in a much more uniformly expanded lung in the prone position.

REGIONAL LUNG VOLUME DISTRIBUTIONS

The early use of CT to investigate mechanical behavior of the lung used single-slice images from patients with acute lung injury at different static distending pressures and examined changes in aeration to characterize recruitment behavior. These pioneering studies were limited by radiation exposure and slow imaging technology to sampling a few lung locations (2,4). Subsequent studies, which took advantage of high-speed scanning during brief breath holds, examined whole-lung and lobar changes in air and tissue volumes (42–44).

The importance of imaging the entire lung for accurate assessment of heterogeneous regional behavior has been shown for patient data (45) and may be seen in the following animal example. In this study, anesthetized mechanically ventilated dogs had contiguous CT images obtained, covering the entire lung from apex to base, acquired one image/breath at end-expiration during steady-state ventilation before and after lung injury with infused oleic acid. Images were calibrated in units of fractional air content (% air) by using air and tissue measurements from each data set. This procedure was repeated at increasing levels of positive end-expiratory pressure (PEEP) and in prone and supine postures. Data are presented as axial (apex to base) profiles of cross-sectional slice volume and corresponding average slice den-

sity (Figure 6). These profiles show distinctly different distributions of volume and aeration throughout the lung. The effect of the weight of the heart and abdominal contents is seen in the shape of the supine curves at low PEEP levels, with a deeper “notch” in the midlung from the heart and a shorter lung with steeper contour of the diaphragm, but the apical area is minimally affected, even with increasing PEEP. This volume distribution translates into a density pattern in which there is normal density in the lung apex, with severe and progressive aeration loss toward the base. Increasing PEEP recruits the midlung first, and even at 20 cm H₂O of PEEP, the caudal base is not fully expanded. Conversely, volume and corresponding density profiles of the prone position show a more elongated, very uniformly expanded lung that increases its aeration throughout with each PEEP increment. The whole-lung pressure-volume curve, partitioned into total, air, and tissue components from CT data (Figure 7), shows none of this regional heterogeneity. Although total air volume was slightly greater supine at every PEEP (probably reflecting progression of injury over time because the supine position was imaged first in this study), arterial blood Po₂ for the prone position was double that in the supine position at functional residual capacity. Similar differences in the vertical distribution of aeration and recruitment with PEEP between positions also were seen. Thus, even static distributions of lung aeration, when whole-lung images can be analyzed, provide a wealth of

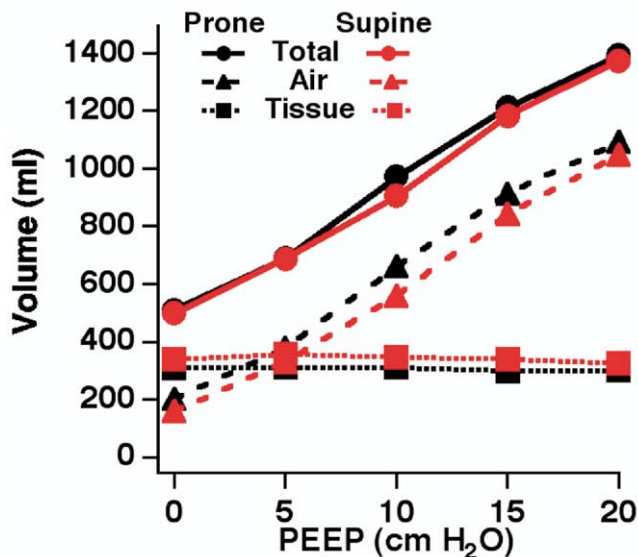


Figure 7. CT pressure-volume curves for the entire lung, determined by summing the individual slice contributions partitioned into air and tissue components for the dog from Figure 6.

information about regional differences in lung mechanical behavior.

3D IMAGE REGISTRATION

To follow up quantitative changes in lung structure and function over time or across different conditions

(such as inflation) or compare with other subjects, images need to be aligned or registered. Registration typically involves identifying and aligning common anatomic landmarks or other image features and then locally expanding or shrinking (warping) the intervening tissue so that mapping of one image to the other is defined (Figure 8) (16). This process, developed for purposes of following up subtle changes in images over time or facilitating quantitative comparisons of individual images with a “standard” (16), has an important corollary for regional lung mechanics. The mathematical transform that defines mapping of the lung from one volume to the other also permits calculation of local lung expansion or contraction on a voxel-by-voxel basis (15). Thus, given two sets of volumetric lung images at two volumes, a 3D image may be produced in which colors (or values) represent local lung volume expansion between the two states (Figure 9). In these slices from a healthy animal imaged at different static pressures in both the prone and supine postures, it easily can be seen that: (1) the lung is most compliant at the lower distending pressures (largest volume changes for the same pressure steps), (2) expansion in the prone position is more uniform than in the supine position, and (3) volume expansion is small, but uniform, in both positions at the greatest distending pressure. With images gated to inspiration and expiration during tidal breathing and assuming, as before, that volume expansion in the lung is realized by the influx of fresh gas, this regional lung expansion

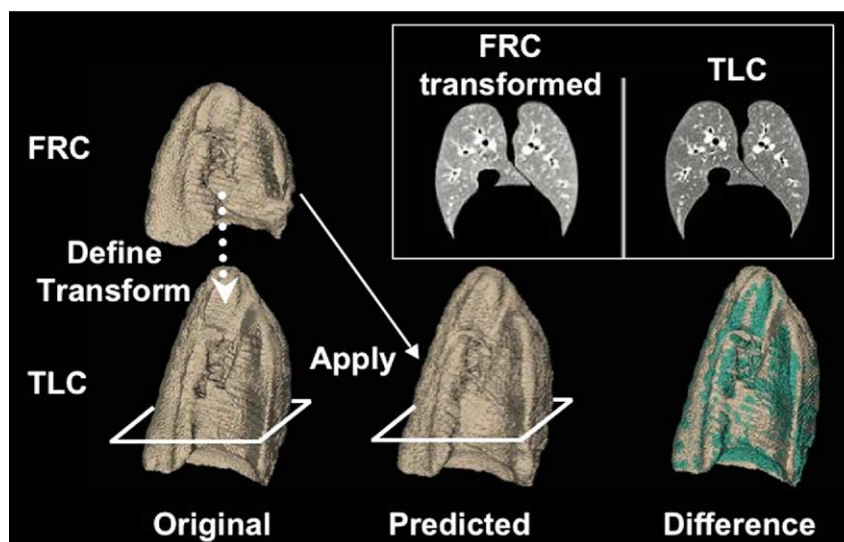


Figure 8. Illustration of registration process mapping the lung at functional residual capacity (FRC) to total lung capacity (TLC). Inset shows an individual slice at FRC transformed to match the corresponding slice at TLC. Reprinted with permission from Joseph Reinhardt and Gary Christensen, University of Iowa.

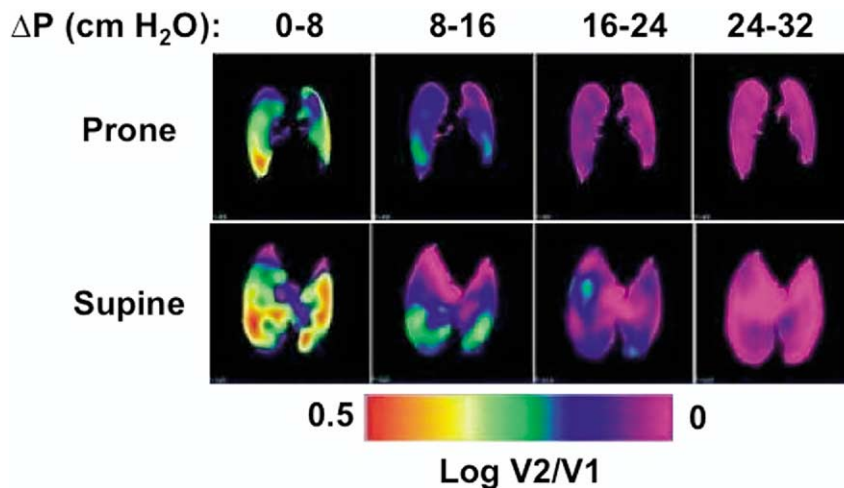


Figure 9. Regional lung expansion of a healthy sheep lung over several pressure steps in both prone and supine positions, determined from the registration transform function. Note that at every pressure step, the lung expands more uniformly in the prone position, and greater expansion occurs for the same pressure step (ie, the lung is more compliant) at lower pressures. Reprinted with permission from Gary Christensen and Joseph Reinhardt, University of Iowa.

analysis can provide another surrogate for regional ventilation. Furthermore, these data are available at high spatial resolution with full 3D localization and tremendous depth of information, including directional strains. As the analysis becomes more automated, application of volumetric determination of regional lung mechanics and ventilation from simple paired CT images will open the door for a new level of understanding of lung regional mechanical function.

CHALLENGES FOR THE FUTURE

CT-based measurements of regional ventilation and lung mechanics are available now, using readily available technology and image analysis tools. The important challenges to widespread adoption of these methods for use in patients include reduction of radiation dose, decreasing image acquisition times, and improving processing speed. Concomitant with these advances need to be parallel advances in data organization, visualization, and parameterization so that results of these studies become useful for answering important scientific and diagnostic questions.

ACKNOWLEDGMENT

The author thanks the organizers of the 2004 International Workshop on Pulmonary Imaging at Penn for the invitation to present and for organizing this special pro-

ceedings issue; Matt Fuld, Dr Blaine Easley, and Dr Ana Fernandez of the Department of Anesthesiology and Critical Care Medicine at the Johns Hopkins University and Jered Sieren, Osama Saba, and Deokiee Chon of the Department of Radiology, Division of Physiological Imaging, University of Iowa, for assistance performing the original studies, data analysis, and figure preparation presented; and Yan Pan, Dinesh Kumar, and Drs Gary E. Christensen and Joseph M. Reinhardt of the University of Iowa for providing data and figures on image registration and regional expansion analysis (Figures 8 and 9).

REFERENCES

- Gattinoni L, Caironi P, Pelosi P, et al. What has computed tomography taught us about the acute respiratory distress syndrome? *Am J Respir Crit Care Med* 2001; 164:1701-1711.
- Gattinoni L, Pesenti A, Avalli L, et al. Pressure-volume curve of total respiratory system in acute respiratory failure. *Computed tomographic scan study. Am Rev Respir Dis* 1987; 136:730-736.
- Gattinoni L, Presenti A, Torresin A, et al. Adult respiratory distress syndrome profiles by computed tomography. *J Thorac Imaging* 1986; 1:25-30.
- Gattinoni L, Mascheroni D, Torresin A, et al. Morphological response to positive end expiratory pressure in acute respiratory failure. *Computerized tomography study. Intensive Care Med* 1986; 12:137-142.
- Bone RC. The ARDS lung: new insights from computed tomography. *JAMA* 1993; 269:2134-2135.
- Engel LA. Intraregional gas mixing and distribution. In: Engel LA, Paiva M, eds. *Gas Mixing and Distribution in the Lung*. 1st Ed. New York: Dekker, 1985; 287-358.
- Hlastala MP. Multiple inert gas elimination technique. *J Appl Physiol* 1984; 56:1-7.

8. Ball WC, Stewart PB, Newsham LGS, et al. Regional pulmonary function studied with xenon 133. *J Clin Invest* 1962; 41:519-531.
9. Murata K, Harumi I, Senda M, et al. Ventilation imaging with positron emission tomography and nitrogen 13. *Radiology* 1986; 158:303-307.
10. Suga K. Technical and analytical advances in pulmonary ventilation SPECT with xenon-133 gas and Tc-99m-Technegas. *Ann Nucl Med* 2002; 16:303-310.
11. Guenther D, Hanisch G, Kauczor HU. Functional MR imaging of pulmonary ventilation using hyperpolarized noble gases. *Acta Radiol* 2000; 41:519-528.
12. Gur D, Drayer BP, Borovetz HS, et al. Dynamic computed tomography of the lung: regional ventilation measurements. *J Comput Assist Tomogr* 1979; 3:749-753.
13. Chevrolet JC, Emrich J, Martin RR, et al. Voluntary changes in ventilation distribution in the lateral posture. *Respir Physiol* 1979; 38:313-323.
14. Kety SS. The theory and applications of the exchange of inert gas at the lungs and tissues. *Pharmacol Rev* 1951; 3:1-41.
15. Pan Y, Kumar D, Hoffman EA, et al. Estimation of regional lung expansion via 3D image registration. *Proc SPIE*. 2005; 5746:453-464.
16. Li B, Christensen GE, Hoffman EA, et al. Establishing a normative atlas of the human lung: intersubject warping and registration of volumetric CT images. *Acad Radiol* 2003; 10:255-265.
17. Otis AB, McKerrow CB, Bartlett RA, et al. Mechanical factors in distribution of pulmonary ventilation. *J Appl Physiol* 1956; 8:427-442.
18. Mead J. Contribution of compliance of airways to frequency-dependent behavior of lungs. *J Appl Physiol* 1969; 26:670-673.
19. Brown RH, Herold CJ, Hirshman CA, et al. Individual airway constrictor response heterogeneity to histamine assessed by high-resolution computed tomography. *J Appl Physiol* 1993; 74:2615-2620.
20. Gur D, Shabason L, Borovetz HS, et al. Regional pulmonary ventilation measurements by xenon enhanced dynamic computed tomography: an update. *J Comput Assist Tomogr* 1981; 5:678-683.
21. Marcucci C, Nyhan D, Simon BA. Distribution of pulmonary ventilation using Xe-enhanced computed tomography in prone and supine dogs. *J Appl Physiol* 2001; 90:421-430.
22. Hoffman EA, Tajik JK, Kugelmass SD. Matching pulmonary structure and perfusion via combined dynamic multislice CT and thin-slice high-resolution CT. *Comput Med Imaging Graphics* 1995; 19:101-112.
23. Tajik JK, Tran BQ, Hoffman EA. Xenon enhanced CT imaging of local pulmonary ventilation. *Proc SPIE* 1996; 2709:40-54.
24. Simon BA, Marcucci C, Fung M, et al. Parameter estimation and confidence intervals for Xe-CT ventilation studies: a Monte Carlo approach. *J Appl Physiol* 1998; 84:709-716.
25. Tajik JK, Chon D, Won C, et al. Subsecond multisection CT of regional pulmonary ventilation. *Acad Radiol* 2002; 9:130-146.
26. Foley WD, Haughton VM, Schmidt J, et al. Xenon contrast enhancement in computed body tomography. *Radiology* 1978; 129:219-220.
27. Winkler SS, Holden JE, Sackett JF, et al. Xenon and krypton as radiographic inhalation contrast media with computerized tomography: preliminary note. *Invest Radiol* 1977; 12:19-20.
28. Kearfott KJ, Rottenberg DA, Deck MDF. Optimization of xenon-enhanced CT studies: beam energy, enhancement, root mean square deviation, and repeatability. *AJNR Am J Neuroradiol* 1982; 4:195-199.
29. Jones AT, Hansell DM, Evans TW. Pulmonary perfusion quantified by electron-beam computed tomography: effects of hypoxia and inhaled NO. *Eur Respir J* 2003; 21:855-861.
30. Tajik JK, Tran BQ, Hoffman EA. New technique to quantitate regional pulmonary microvascular transit times from dynamic X-ray CT images. *SPIE Med Imaging Physiol Funct Multidimensional Images* 1998; 3337: 24-32.
31. Yonas H, Good WF, Gur D, et al. Mapping cerebral blood flow by xenon-enhanced computed tomography: clinical experience. *Radiology* 1984; 152:435-442.
32. Kalender WA, Polacin A, Eidloth H, et al. Brain perfusion studies by xenon-enhanced CT using washin/washout study protocols. *J Comput Assist Tomogr* 1991; 15:816-822.
33. Kreck TC, Krueger MA, Altemeier WA, et al. Determination of regional ventilation and perfusion in the lung using xenon and computed tomography. *J Appl Physiol* 2001; 91:1741-1749.
34. Wood LD, Bryan AC, Bau SK, et al. Effect of increased gas density on pulmonary gas exchange in man. *J Appl Physiol* 1976; 41:206-210.
35. Cullen SC, Eger EI, Cullen BF, et al. Observations on the anesthetic effect of the combination of xenon and halothane. *Anesthesiology* 1969; 31:305-309.
36. Yonas H, Grundy B, Gur D, et al. Side effects of xenon inhalation. *J Comput Assist Tomogr* 1981; 5:591-592.
37. Lachmann B, Armbruster S, Schairer W, et al. Safety and efficacy of xenon in routine use as an inhalational anaesthetic. *Lancet* 1990; 335: 1413-1415.
38. Gattinoni L, Pelosi P, Crotti S, et al. Effects of positive end-expiratory pressure on regional distribution of tidal volume and recruitment in adult respiratory distress syndrome. *Am J Respir Crit Care Med* 1995; 151:1807-1814.
39. Victorino JA, Borges JB, Okamoto VN, et al. Imbalances in regional lung ventilation: a validation study on electrical impedance tomography. *Am J Respir Crit Care Med* 2004; 169:791-800.
40. Simon BA. Non-invasive imaging of regional lung function using X-ray computed tomography. *J Clin Monit* 2000; 16:433-442.
41. Fuld MK, Easley RB, Saba OI, et al. Regional specific compliance as a surrogate measure for regional specific ventilation in supine sheep [abstract]. *Am J Respir Crit Care Med* 2004; 169:547A.
42. Puybasset L, Cluzel P, Gusman P, et al. Regional distribution of gas and tissue in acute respiratory distress syndrome. I. Consequences for lung morphology. *CT Scan ARDS Study Group. Intensive Care Med* 2000; 26:857-869.
43. Vieira SRR, Puybasset L, Lu Q, et al. A scanographic assessment of pulmonary morphology in acute lung injury. *Am J Respir Crit Care Med* 1999; 159:1612-1623.
44. Vieira SR, Puybasset L, Richecoeur J, et al. A lung computed tomographic assessment of positive end-expiratory pressure-induced lung overdistension. *Am J Respir Crit Care Med* 1998; 158:1571-1577.
45. Lu Q, Malbouisson LM, Mourgeon E, et al. Assessment of PEEP-induced reopening of collapsed lung regions in acute lung injury: are one or three CT sections representative of the entire lung? *Intensive Care Med* 2001; 27:1504-1510.